# Preparation and characterization of 18650 Li(Ni$_{1/3}$Co$_{1/3}$Mn$_{1/3}$)O$_2$/graphite high power batteries

Yan-Bing He [a],[*], Zhi-Yuan Tang [a], Quan-Sheng Song [a], Hui Xie [a], Quan-Hong Yang [a], Yuan-Gang Liu [b], Guo-Wei Ling [a]

[a] Department of Applied Chemistry, School of Chemical Engineering and Technology, Tianjin University, Tianjin 300072, China
[b] McNair Technology Co., Ltd., Dongguan, Guangdong 523700, China

## ARTICLE INFO

## ABSTRACT

The commercial 18650 Li(Ni$_{1/3}$Co$_{1/3}$Mn$_{1/3}$)O$_2$/graphite high power batteries were prepared and their electrochemical performance at temperatures of 25 and 50 °C was extensively investigated. The results showed that the charge-transfer resistance ($R_{ct}$) and solid electrolyte interface resistance ($R_{sei}$) of the high power batteries at 25 °C decreased as states of charge (SOC) increased from 0 to 60%, whereas $R_{ct}$ and $R_{sei}$ increased as SOC increased from 60 to 100%. The discharge plateau voltage of batteries reduced greatly with the increase in discharge rate at both 25 and 50 °C. The high power batteries could be discharged at a very wide current range to deliver most of their capacity and also showed excellent power cycling performance with discharge rate of as high as 10 C at 25 °C. The elevated working temperature did not influence the battery discharge capacity and cycling performance at lower discharge rates (*e.g.* 0.5, 1, and 5 C), while it resulted in lower discharge capacity at higher discharge rates (*e.g.* 10 and 15 C) and bad cycling performance at discharge rate of 10 C. The batteries also exhibited excellent cycle performance at charge rate of as high as 8 C and discharge rate of 10 C.

© 2008 Elsevier B.V. All rights reserved.

## 1. Introduction

There are many studies about high power lithium-ion batteries used as power sources for hybrid electric vehicles (HEVs) and power tools [1,2]. At present, the applications of lithium-ion batteries in the HEV systems and power tools are limited by their cycling performance, thermal abuse characteristics, and high cost. The LiCoO$_2$ cathode materials show high energy density and excellent cycling stability, but they also have some disadvantages such as poor thermal stability, inferior overcharge characteristics, and environmental pollution problems. These disadvantages limit the use of LiCoO$_2$ materials in large capacity and high power lithium-ion batteries [3–8].

The cathode materials of spinel LiMn$_2$O$_4$ and olivine LiFePO$_4$ exhibit excellent overcharge characteristics and good thermal stability, which make them promising for the use in large capacity and high power lithium-ion batteries. However, there are also some limitations for spinel LiMn$_2$O$_4$ and olivine LiFePO$_4$. It is well known that the energy density of the two materials is lower than that of LiCoO$_2$. For the spinel LiMn$_2$O$_4$, another obstacle is its poor structure stability during the battery cycling process, espe-

cially during the operation at elevated temperatures. Meanwhile, LiMn$_2$O$_4$-based cathode also suffers from significant capacity loss and impedance increase, which is attributed to Mn dissolution induced by HF in the electrolyte [9–12]. For LiFePO$_4$, the synthesis process is usually difficult and time-consuming. The LiFePO$_4$ is characterized by the low conductivity, mainly resulted from the low lithium-ion diffusion rate and low electronic conductivity [13,14]. Moreover, the preparation and coating of LiFePO$_4$ slurry on an aluminum foil collector are also difficult.

Layered Li(Ni$_{1/3}$Co$_{1/3}$Mn$_{1/3}$)O$_2$ materials, which possess large specific capacity and excellent safety characteristics due to much lower heat generation, are very promising for use as the positive electrode in lithium-ion batteries. The layered Li(Ni$_{1/3}$Co$_{1/3}$Mn$_{1/3}$)O$_2$ materials can be synthesized by various methods [15–25]. The electrochemical performance of these materials was mainly investigated by using coin cells. It is well-known that the safety performance of layered Li(Ni$_{1/3}$Co$_{1/3}$Mn$_{1/3}$)O$_2$ is better than that of LiCoO$_2$ [3,26], making it suitable to be used as cathode materials for commercial lithium-ion high power batteries [27]. However, so far there are few studies on the preparation and electrochemical performance of commercial Li(Ni$_{1/3}$Co$_{1/3}$Mn$_{1/3}$)O$_2$/graphite high power batteries.

In this paper, the layered Li(Ni$_{1/3}$Co$_{1/3}$Mn$_{1/3}$)O$_2$ material was synthesized through a soft chemical process with a subsequent heat treatment. The commercial 18650 Li(Ni$_{1/3}$Co$_{1/3}$Mn$_{1/3}$)O$_2$/graphite

* Corresponding author. Tel.: +86 769 83015365.
E-mail address: hezuzhang_2000@163.com (Y.-B. He).

high power batteries were prepared and their electrochemical performance was studied. The high power batteries show excellent rate-discharge and cycling performance.

## 2. Experimental

The layered structure $Li(Ni_{1/3}Co_{1/3}Mn_{1/3})O_2$ was synthesized by the co-precipitation method as follows. 0.25 M aqueous solution of the metal nitrates was prepared with a cation ratio of Ni:Co:Mn = 1:1:1. The preparation of $M(OH)_2$ ($M$ = Ni, Co, Mn) was achieved by slowly dripping the nitrate solution and 0.5 M NaOH solution synchronously into a glass reactor with continuous stirring. The pH value of the reactant solution was adjusted by ammonia and was kept at 11. The $M(OH)_2$ precipitate was filtrated, washed, dried and mixed with stoichiometric amount of $LiOH \cdot H_2O$. The mixed powder was ground in an automatic grinder and was pressed into pellets. The pellets were initially heat-treated at 500 °C for 5 h for the impregnation of LiOH into the matrix. The product was then cooled and re-ground, and the obtained pellets were heat-treated at 1000 °C for 12 h, followed by quenching to room temperature.

X-ray diffraction (XRD) patterns of the samples were obtained by a PANAlytical X'Pert powder diffractometer using Co Kα radiation in an angular range of 10–90° ($2\theta$) with a 0.02° ($2\theta$) step. The structural parameters were calculated by using the MDI Jade 5.0 profile matching refinement method for the XRD diagrams. The microstructure and morphology of the prepared powders was observed by using an environment scanning electron microscope (Philips XL-30 ESEM).

18650 lithium-ion batteries (18 mm in diameter and 65 mm in height) were assembled. The nominal capacity of the batteries was designed to be 1300 mAh. The batteries used the prepared layered $Li(Ni_{1/3}Co_{1/3}Mn_{1/3})O_2$ as cathodes, graphite as anodes, and polyethylene as separator. The $Li(Ni_{1/3}Co_{1/3}Mn_{1/3})O_2$ cathodes consisted of 86 wt% $Li(Ni_{1/3}Co_{1/3}Mn_{1/3})O_2$, 9 wt% conductive graphite, and 5 wt% poly(vinylidene fluoride) (PVDF). The graphite anodes consisted of 91 wt% composite graphite, 6 wt% styrene-butadiene rubber (SBR), and 3 wt% carboxymethyl cellulose (CMC). 1 M $LiPF_6$ in a 1:1:1 mixture of ethylene carbonate, dimethyl carbonate and ethylene methyl carbonate (1 M $LiPF_6$/EC + DMC + EMC) was used as the electrolyte.

Positive electrodes were obtained by coating the mixing slurry of $Li(Ni_{1/3}Co_{1/3}Mn_{1/3})O_2$ active material, conductive graphite, and PVDF onto an aluminum foil collector. The loading amount of the cathode material on each side of the electrodes was about 10 mg cm$^{-2}$. Negative electrodes were prepared by coating the mixing slurry of composite graphite, SBR and CMC onto a copper foil. The loading amount of the anode material on each side of the electrodes was about 5 mg cm$^{-2}$. The injection of the electrolyte was conducted in an argon filled glove box.

The formation, rate-discharge and cycle performance tests of batteries were performed by using the BS-9300 and BS-9366 lithium-ion battery testers. Since the most recent industrial formation process includes only one cycle, the experimental batteries in this study also underwent one cycle of charge–discharge for formation. The batteries were charged with a constant current of 65 mA (0.05 C) to 3.00 V, 130 mA (0.1 C) to 3.85 V, and 260 mA (0.2 C) to 4.20 V, respectively, followed by holding the voltage at 4.20 V until the current dropped to 13 mA (0.01 C), and then the batteries were discharged at 650 mA (0.5 C) to a cut-off voltage of 2.75 V. After formation, all batteries were charged and discharged three times between 2.75 and 4.20 V at 650 mA (0.5 C) to stabilize the performance of batteries. The rate-discharge and cycle performance of batteries was examined between 2.75 and 4.20 V at temperatures of 25 and 50 °C. The surface temperature of batteries was recorded during the rate-discharge performance testing. A type-K thermal couple was attached to the center of the largest face of the batteries to record the temperature change.

The electrochemical working station (Gamry Instrument model PCI 4-750) was used to measure the electrochemical impedance spectrum (EIS) of the 18650 $Li(Ni_{1/3}Co_{1/3}Mn_{1/3})O_2$/graphite high power batteries. It was necessary that one nickel lead was welded on the cathode and the other on the anode of 18650 battery shell before the EIS testing. Then the batteries were connected with the electrochemical working station to test the EIS of batteries. The EIS of batteries with different states of charge (SOC) at a temperature of 25 °C was measured at the open circuit voltage (OCV) of the batteries with $Li(Ni_{1/3}Co_{1/3}Mn_{1/3})O_2$ cathodes as the working electrode and graphite anodes as both the reference and counter electrodes. To describe SOC of the batteries, we defined it as the ratio of the charging capacity at a specific point to the capacity obtained at 25 °C by charging at 0.5 C from the fully discharged state to 4.2 V. For the measurement of the impedance at various SOC, the experiments were started from the fully discharged state. The batteries were charged at 0.5 C to a specific SOC and kept for 0.5 h in the oven with a temperature of 25 °C to reach a stable OCV. The impedance was measured by applying a 5 mV of ac oscillation with the frequency ranging from 100 kHz to 0.01 Hz. This procedure was repeated until the batteries were fully charged.

## 3. Results and discussion

Fig. 1 shows the XRD patterns of $Li(Ni_{1/3}Co_{1/3}Mn_{1/3})O_2$ materials, such as as-prepared one, the discharged one (2.75 V) and the charged one (4.2 V). In all cases, the observed diffraction lines can be indexed based on the $R$-$3m$ space group and are consistent with the layered structure of α-NaFeO$_2$. The 3d metals (Ni, Co, and Mn) are supposed to be randomly distributed on the (3b) crystallographic position, whereas the lithium atoms occupy the (3a) sites between the metallic slabs. The hexagonal lattice parameters for the respective materials are $a$ = 2.8719 Å, $c$ = 14.2628 Å for the as-prepared $Li(Ni_{1/3}Co_{1/3}Mn_{1/3})O_2$; $a$ = 2.8633 Å, $c$ = 14.3017 Å for $Li(Ni_{1/3}Co_{1/3}Mn_{1/3})O_2$ cathode discharged to 2.75 V; and $a$ = 2.8240 Å, $c$ = 14.4892 Å for $Li(Ni_{1/3}Co_{1/3}Mn_{1/3})O_2$ cathode charged to 4.2 V. An expansion of the c parameter and a shrinkage a parameter of the delithiated material are observed as compared with the fully lithiated material.
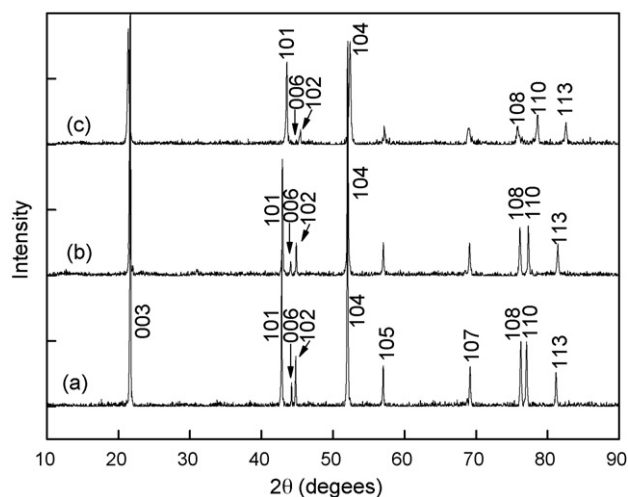


**Fig. 1.** XRD patterns of: (a) as-prepared $Li(Ni_{1/3}Co_{1/3}Mn_{1/3})O_2$; (b) $Li(Ni_{1/3}Co_{1/3}Mn_{1/3})O_2$ discharged to 2.75 V and (c) $Li(Ni_{1/3}Co_{1/3}Mn_{1/3})O_2$ charged to 4.2 V.

There are four major different XRD characteristics for the charged $Li(Ni_{1/3}Co_{1/3}Mn_{1/3})O_2$ compared with discharged one: (1) the (006) line almost disappears from the XRD patterns of the delithiated (charged) $Li(Ni_{1/3}Co_{1/3}Mn_{1/3})O_2$; (2) the (108) and (110) peaks for the delithiated $Li(Ni_{1/3}Co_{1/3}Mn_{1/3})O_2$ are clearly separated by $2°$ $(2\theta)$; (3) the (101), (102), (104), (110) and (113) lines for the delithiated $Li(Ni_{1/3}Co_{1/3}Mn_{1/3})O_2$ are shifted toward the higher $2\theta$ angles; and (4) the peak intensity of the delithiated $Li(Ni_{1/3}Co_{1/3}Mn_{1/3})O_2$ becomes weaker. These results show that the microstructure of $Li(Ni_{1/3}Co_{1/3}Mn_{1/3})O_2$ makes some changes from changed to discharged state.

Fig. 2 shows the SEM micrographs of the as-prepared $Li(Ni_{1/3}Co_{1/3}Mn_{1/3})O_2$. The powders consist of spherical particles with an average diameter of 6–10 $\mu m$, and the spherical particles are composed of agglomerates of much smaller primary particles. The materials show the highly ordered layered structure and well defined secondary and primary particles. This kind of particle morphology is common for samples produced by co-precipitation of mixed transition metal hydroxides followed by calcination with a lithium compound. The smaller primary particles are helpful for improving the high power performance of the material.

The EIS technique is a very powerful tool to analyze electrode reactions and has been widely used to examine the electrochemical $Li^+$ intercalation into carbonaceous materials and deintercalation from cathode materials [28–30]. As shown in Fig. 3, the EIS of

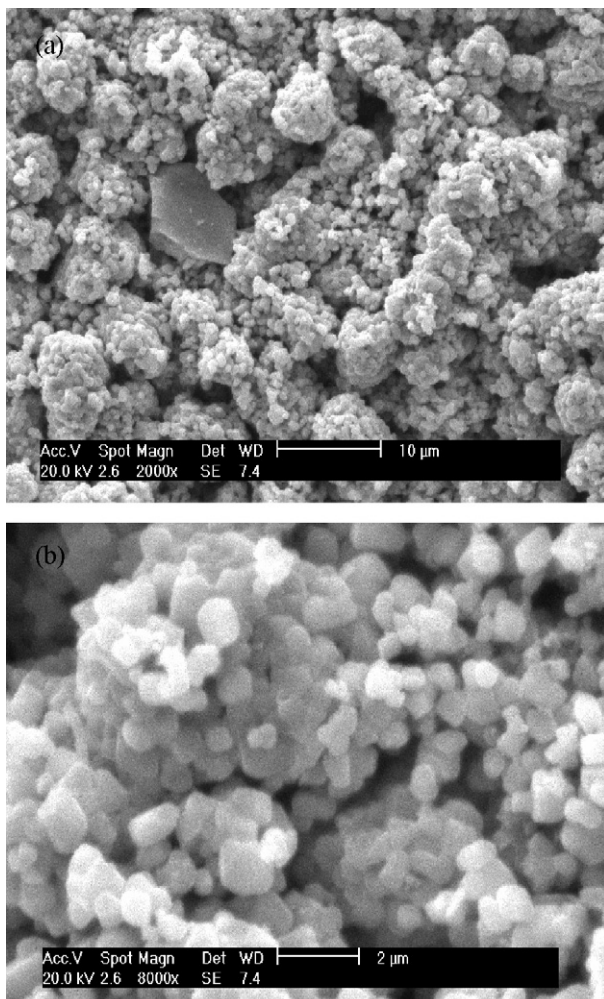**Fig. 3.** EIS of 18650 $Li(Ni_{1/3}Co_{1/3}Mn_{1/3})O_2$/graphite high power batteries with 100% SOC at 25 °C.

the 18650 $Li(Ni_{1/3}Co_{1/3}Mn_{1/3})O_2$/graphite high power batteries shows an inductive loop at very high frequency followed by two over-lapped semicircles at high to middle frequency and a slope line at low frequency. The inductive loop at very high frequency, which is affected by the battery and electrode structure, could be attributed to the jelly-roll configuration and porous electrode structure of 18650 batteries [31]. After deleting the inductive loop, the impedance spectra of 18650 batteries at various SOC are shown in Fig. 4. These impedance patterns can be interpreted in terms of bulk impedance, interfacial impedance and faradic impedance [31]. The intersection of the diagram with real axis refers to a bulk resistance. The bulk impedance could be a pure ohmic resistance ($R_b$), which reflects the electronic and ionic resistance of two electrodes and electrolyte/separator, and of other resistive components such as current collectors, nickel leads and the contact resistance between the electrochemical working station and nickel lead. The interfacial impedance, which corresponds to the semicircle at high frequency, could be attributed to the resistance ($R_{sei}$) and capacitance ($C_{sei}$) of the solid electrolyte interface formed on the surface of two electrodes. The faradic impedance consists of charge-transfer impedance and Warburg impedance. The charge-transfer impedance, which corresponds to the semicircle at medium fre-
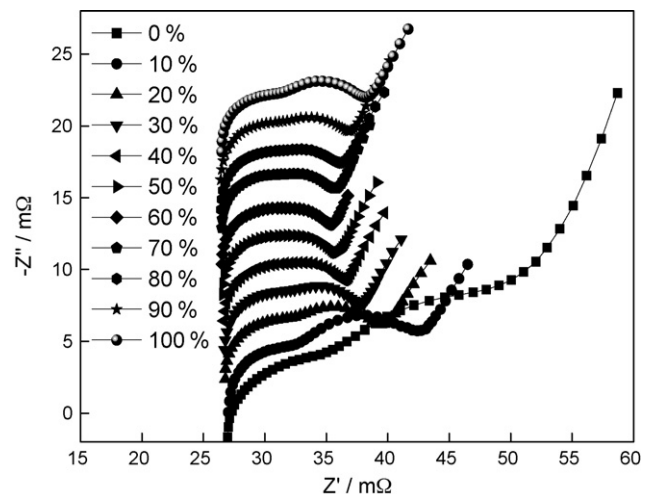
**Fig. 2.** SEM images of as-prepared $Li(Ni_{1/3}Co_{1/3}Mn_{1/3})O_2$: (a) 2000× and (b) 8000×.

**Fig. 4.** EIS of 18650 $Li(Ni_{1/3}Co_{1/3}Mn_{1/3})O_2$/graphite high power batteries with various SOC at 25 °C.
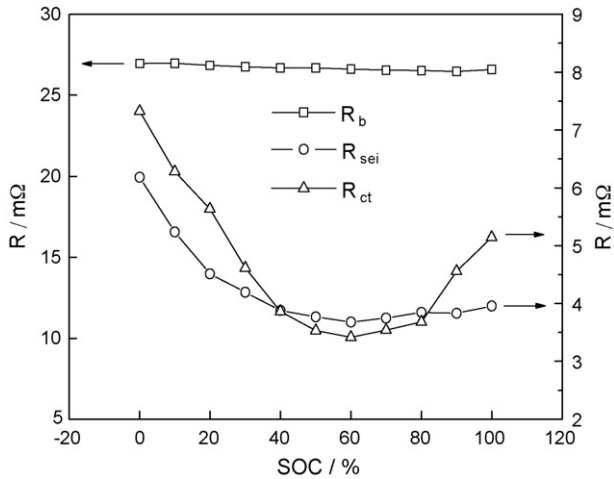
**Fig. 5.** Values of the $R_b$, $R_{sei}$ and $R_{ct}$ obtained by simulating the data of Fig. 4.

quency, could be attributed to the charge-transfer resistance ($R_{ct}$) and its related double-layer capacitance ($C_{dl}$). Warburg impedance, which corresponds to the slope line at low frequency, could be related to the diffusion of lithium ions on the interface between the active material particles and the electrolyte.

Fig. 5 shows the individual values of the $R_b$, $R_{sei}$, and $R_{ct}$ for the EIS of 18650 batteries with different SOC at 25 °C, which were obtained by simulating the EIS data of Fig. 4 using ZSimpWin 3.0 software. The simulation methods and equivalent circuit used to fit the EIS are shown in Fig. 6. It can be seen from Fig. 5 that the $R_b$ is almost independent on SOC; whereas the $R_{sei}$ and $R_{ct}$ decrease as SOC increases from 0 to 60%, and the $R_{sei}$ and $R_{ct}$ increase as SOC increases from 60 to 100%. The $R_{sei}$ change observed from a Li-ion battery can be ascribed to the combined effect of two reverse changes in the respective $R_{sei}$ value of the graphite and cathode [30,31]. Fig. 5 indicates that the $R_{sei}$ change of the graphite and $Li(Ni_{1/3}Co_{1/3}Mn_{1/3})O_2$ cathode cannot be compensated by each other at various SOC of batteries, especially at SOC from 0 to 60%. The change of $R_{ct}$ shows that charging a Li-ion battery from the discharged state is relatively difficult, and this process becomes easier at the charging voltage plateau, and then the charging becomes difficult again after the SOC of 80% where the battery voltage increases greatly. The change in $R_{sei}$ and $R_{ct}$ results in the change in $R_{cell}$. The
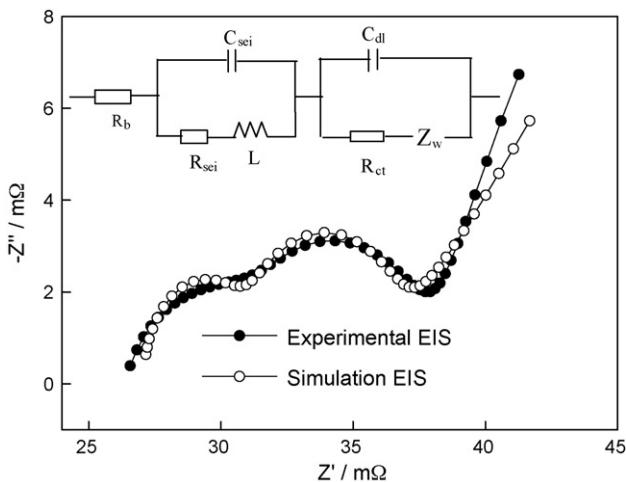


**Fig. 6.** The experimental and simulation EIS data of 18650 high power batteries with 100% SOC at 25 °C and the equivalent circuit used to fit the EIS.
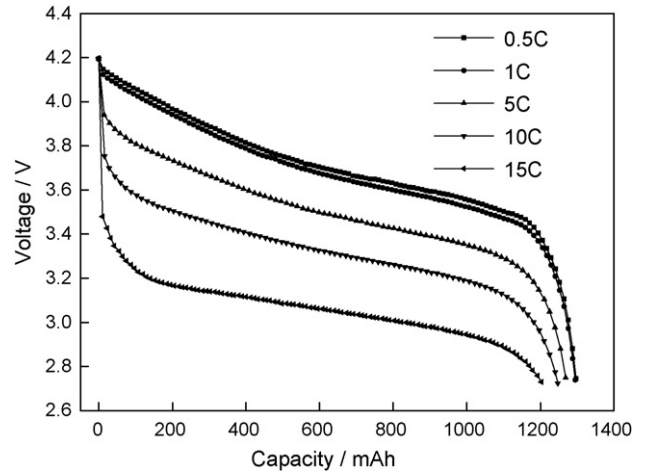


**Fig. 7.** Rate-discharge performance of 18650 $Li(Ni_{1/3}Co_{1/3}Mn_{1/3})O_2$/graphite high power batteries at 25 °C, which were charged at 0.5 C and discharged with rates of 0.5, 1, 5, 10 and 15 C, respectively.

$R_{cell}$ is mainly contributed by $R_b$, $R_{sei}$, and $R_{ct}$. Fig. 5 also shows that the $R_b$ contributes more than half of the total cell resistance ($R_{cell}$) at 25 °C and the value of $R_b$ reaches about 26.5 mΩ. In fact, the internal resistance (pure ohmic resistance) of batteries was also tested by using an internal resistance tester and the value was about 13–15 mΩ. This difference may be attributed to the resistance of the nickel leads and the contact resistance between the electrochemical working station and nickel leads.

Fig. 7 shows the rate-discharge performance of the batteries at 25 °C. All of the batteries were charged at 0.5 C, and then discharged at rates of 0.5, 1, 5, 10 and 15 C, respectively. It can be seen that the discharge voltage is distinctly reduced at the beginning of discharge with discharge rates of 5, 10 and 15 C. The decrease of discharge voltage is more obvious with the increase in discharge rate. The discharge curve shows a minimum voltage at the initial period when the battery is discharged at a high-rate of 15 C, which may be attributed to the large polarization at a high discharge current and the relatively slow lithium-ion diffusion rate in solid phase and electrolyte.

It also can be obtained from Fig. 7 that the discharge capacity of high power batteries at discharge rates of 0.5, 1, 5, 10 and 15 C is 1297.50, 1294.65, 1269.23, 1247.35 and 1202.50 mAh, respectively. The discharge capacity at rates of 5, 10 and 15 C is respective 98.04, 96.34 and 92.88% of that at rate of 1 C. These results show that the high power batteries can be discharged at a very wide range of current to deliver most of their capacity, indicating very good kinetic characteristics for the high power batteries. The excellent rate performance can be attributed to following reasons: the highly ordered layered structure and well defined secondary and primary particles of $Li(Ni_{1/3}Co_{1/3}Mn_{1/3})O_2$ material, the relatively less $R_{ct}$ of batteries, the appropriate loading amount of the $Li(Ni_{1/3}Co_{1/3}Mn_{1/3})O_2$ material on each side of the electrodes and the suitable electrodes thickness.

Fig. 8 shows that the battery temperature gradually increases during high-rate discharge, which can reach respective 41.5, 57.0, and 76.0 °C at the end of discharge for discharge rates of 5, 10, and 15 C, whereas the battery temperature almost does not change during 0.5 and 1 C rate discharge. When a battery is discharged, the value of heat generation can be calculated by the formula of $Q = i^2 R_{cell} t$, where $Q$ represents the heat generation, $i$ for discharge current, $R_{cell}$ for the total cell resistance, and $t$ for time. However, the heat dissipation also occurs during the battery discharge, which is related to the size and shape of batteries. This means that the heat
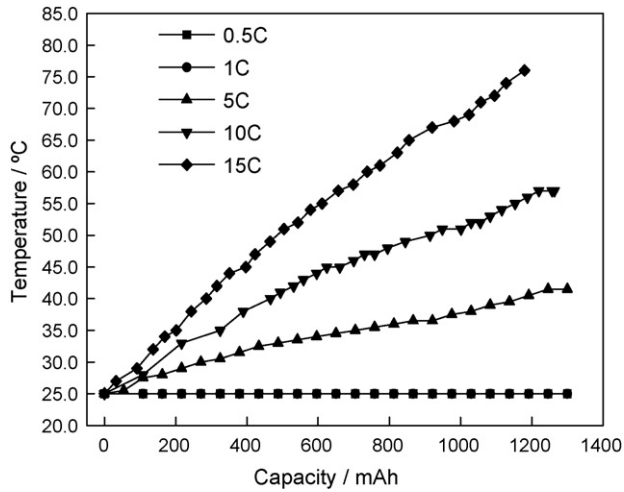
**Fig. 8.** The surface temperature of 18650 Li(Ni$_{1/3}$Co$_{1/3}$Mn$_{1/3}$)O$_2$/graphite high power batteries at 25 °C with various discharge rates of 0.5, 1, 5, 10 and 15 C.
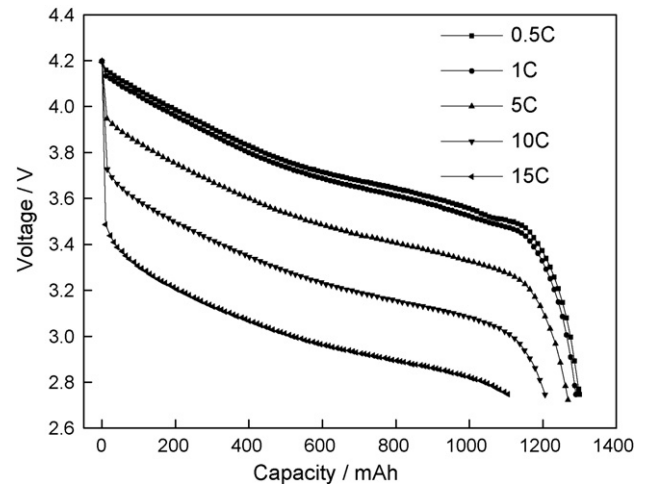


**Fig. 10.** Rate-discharge performance of 18650 Li(Ni$_{1/3}$Co$_{1/3}$Mn$_{1/3}$)O$_2$/graphite high power batteries at 50 °C, which were charged at 0.5 C and discharged with rates of 0.5, 1, 5, 10 and 15 C, respectively.

generation and heat dissipation is a pair of discrepancy. If the heat generation and dissipation are in balance, the temperature of the battery will not change, which occurs only in low-rate discharge. If this balance is broken and the rate of heat generation is higher, the temperature of the battery will rise, which is the case for high-rate discharge.

Fig. 9 reveals a good cycling property of high power batteries with various discharge rates at 25 °C. The value of capacity after 100 cycles at 1 and 5 C discharge is 1247.65 and 1220.58 mAh and the capacity retention is 96.37 and 96.03%, respectively. A discharge capacity of 1209.45 mAh is obtained after 100 cycles even at the high discharge rate of 10 C, which is 96.95% of its initial value. Thus, the 18650 Li(Ni$_{1/3}$Co$_{1/3}$Mn$_{1/3}$)O$_2$/graphite high power batteries show excellent power cycling performance at 25 °C.

Fig. 10 shows the rate-discharge performance of batteries at 50 °C. The discharge capacity of batteries at rates of 0.5, 1, 5, 10 and 15 C is 1300.21, 1290.64, 1269.19, 1206.59 and 1105.11 mAh, respectively. The discharge capacity at rates of 5, 10 and 15 C is respective 98.34, 93.49 and 85.62% of that at rate of 1 C. As compared with the results of Fig. 7, it can be seen that the discharge capacity for the 10 and 15 C rate at 50 °C is less than that for the same rate at 25 °C.

Fig. 11 indicates that the battery temperature gradually increases during the high-rate discharge process at 50 °C, which can reach respective 66.5, 84.0 and 92.0 °C at the end of discharge for rates of 5, 10 and 15 C.

Fig. 12 presents the cycling property of batteries with various discharge rates at 50 °C. The capacity retention after 100 cycles is 96.28% at discharge rate of 1 C, 95.42% at 5 C, and 87.91% at 10 C, respectively. As compared with the results of Fig. 9, it can be observed that the battery cycling property for 1 and 5 C at 50 °C is similar with that for the same rate at 25 °C; whereas the cycling property for 10 C at 50 °C is relatively worse than that for the same rate at 25 °C. These results may be attributed to the elevated battery temperature. It can be seen from Figs. 8 and 11 that the battery temperature increases to 57 °C at the end of 10 C discharge at discharge temperature of 25 °C; whereas it reaches 84 °C at discharge temperature of 50 °C. It is well-known that the electrolyte is more instable at more elevated temperature (>50 °C). The higher temperature results in the thermal decomposition of the electrolyte and the deposition of electrolyte decomposition products on the surface of the graphite [32], which can lead to more SEI film formation on the active material surface [20]. So the polarization at the elevated temperature seems to be more pronounced, which results in the more capacity loss and the relatively
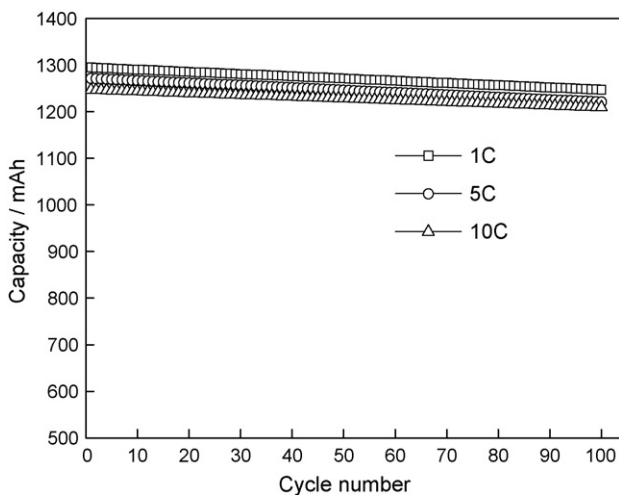


**Fig. 9.** The cycling performance of 18650 Li(Ni$_{1/3}$Co$_{1/3}$Mn$_{1/3}$)O$_2$/graphite high power batteries at 25 °C, which were charged at 0.5 C and discharged with various discharge rates of 1, 5 and 10 C.
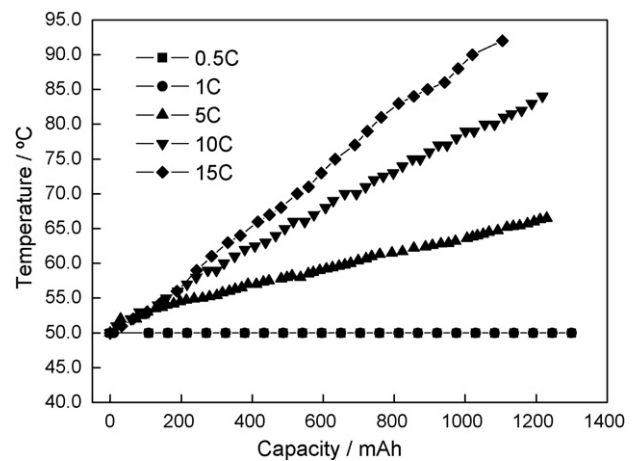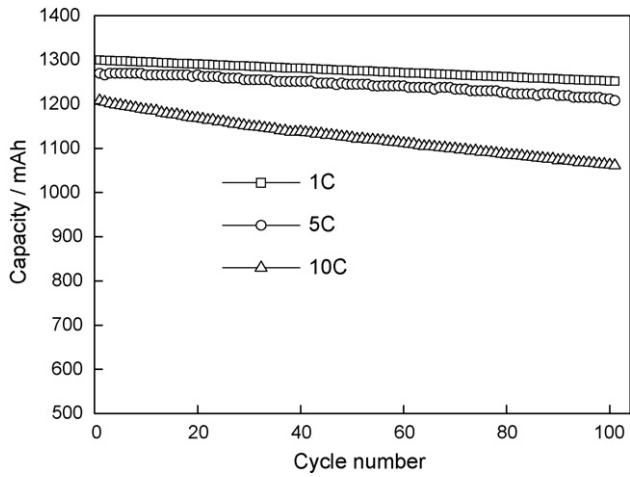


**Fig. 11.** The surface temperature of 18650 Li(Ni$_{1/3}$Co$_{1/3}$Mn$_{1/3}$)O$_2$/graphite high power batteries at 50 °C with various discharge rates of 0.5, 1, 5, 10 and 15 C.
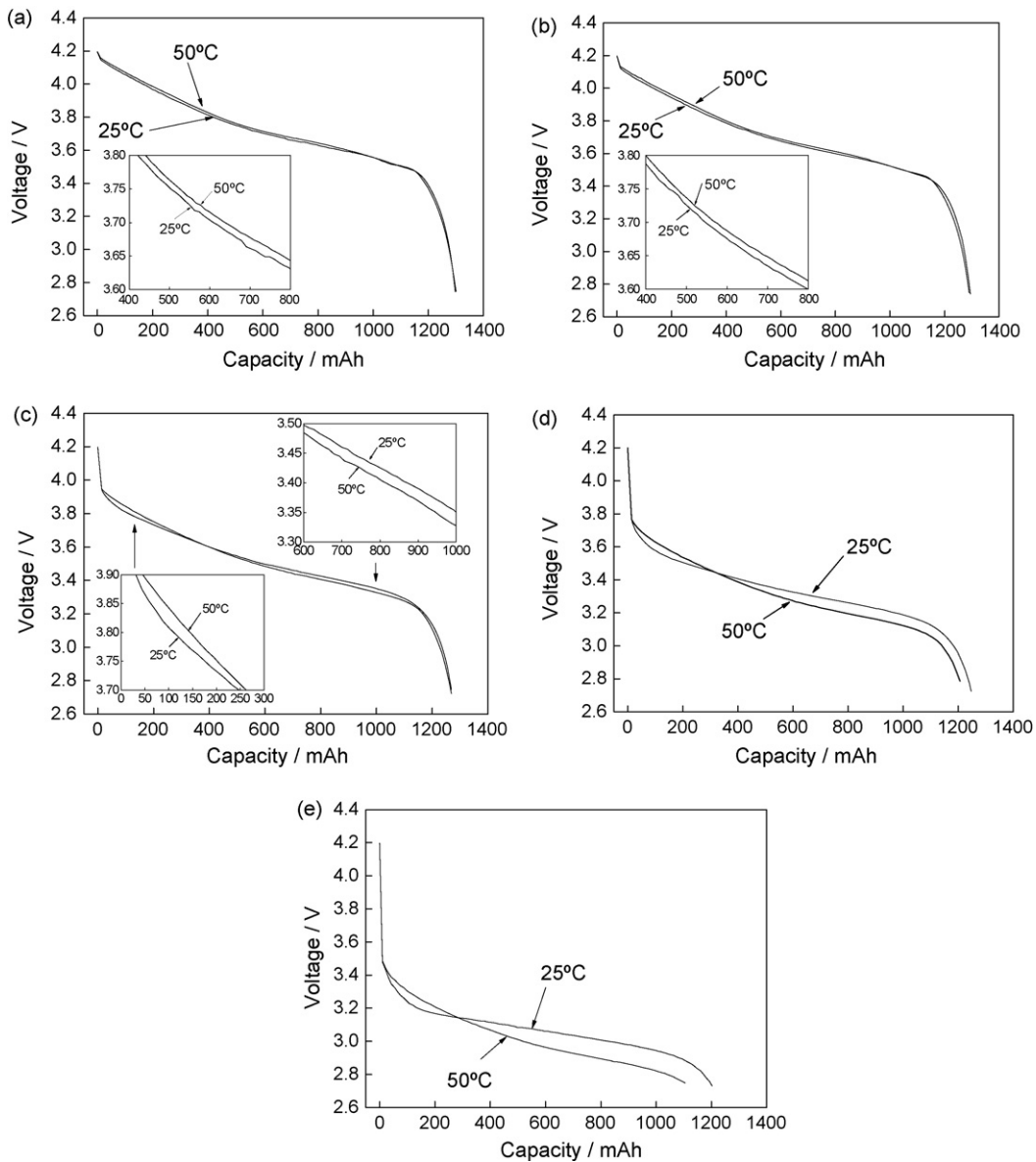
**Fig. 12.** The cycling performance of 18650 Li(Ni$_{1/3}$Co$_{1/3}$Mn$_{1/3}$)O$_2$/graphite high power batteries at 50 °C with various discharge rates of 1, 5 and 10 C.

bad cycling property for discharge rate of 10 C at 50 °C. However, the 18650 Li(Ni$_{1/3}$Co$_{1/3}$Mn$_{1/3}$)O$_2$/graphite high power batteries still show good power cycle performance at 50 °C.

Fig. 13 shows the comparison of discharge voltage of the high power batteries at temperatures of 25 and 50 °C. The change of discharge voltage with the discharge rate at temperatures of 25 and 50 °C is complicated. The discharge voltage plateau for rates of 0.5 and 1 C at 50 °C is higher than that for the same rate at 25 °C during the whole discharge process; whereas the discharge voltage of 5, 10 and 15 C rate at 25 and 50 °C shows different characteristic. It can be seen from Fig. 13(c–e) that the discharge voltage plateau at 50 °C is higher than that at 25 °C at the initial discharge stage; whereas it is lower at later discharge stage. It can also be observed that the discharge capacity of 5, 10 and 15 C rate is about 390, 300 and 250 mAh, respectively, when the discharge voltage at 25 °C is equal to that at 50 °C.

There are two factors which influence the discharge voltage. One is the discharge current, and the other is the battery temperature. The appropriate elevated temperature ($\leq$50 °C) can mainly enhance



**Fig. 13.** The comparison of rate-discharge performance of 18650 Li(Ni$_{1/3}$Co$_{1/3}$Mn$_{1/3}$)O$_2$/graphite high power batteries at temperatures of 25 and 50 °C: (a) 0.5 C; (b)1 C; (c) 5 C; (d); 10 C and (e) 15 C.
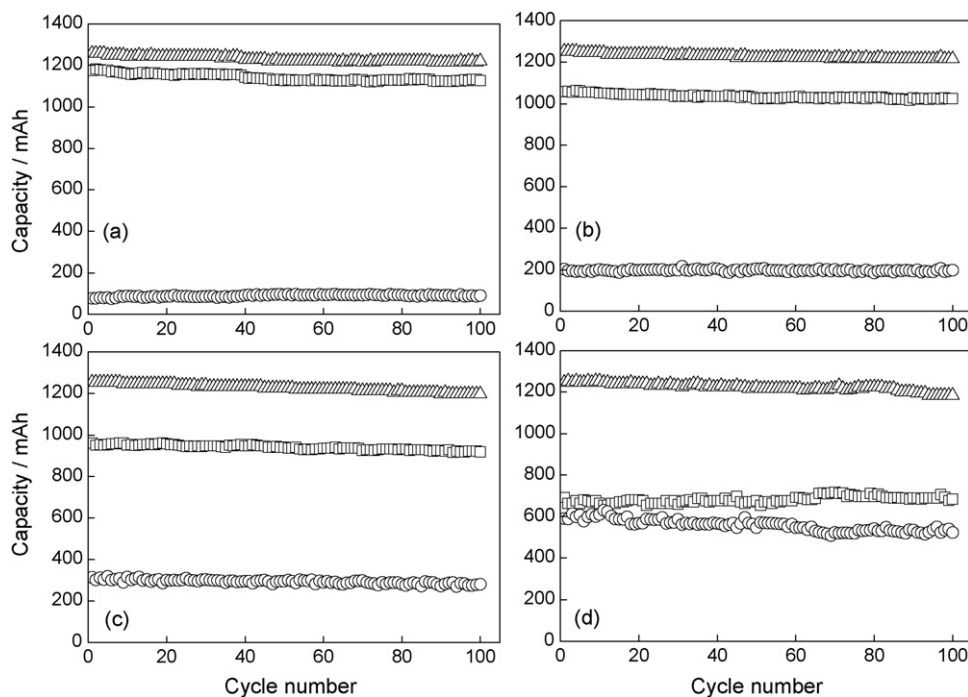
**Fig. 14.** The discharge capacity (△) at discharge rate of 10 C, CC-charge capacity (□) and CV-charge capacity (○) with various charge rates during 100 cycles: (a) 1 C; (b) 3 C; (c) 5 C and (d) 8 C.

the lithium-ion diffusion rate in solid phase and electrolyte, which reduces the concentration polarization and enhances the discharge voltage. The high discharge current can increase the electrochemical polarization, which decreases the discharge voltage.

When the batteries are discharged at low rates (*e.g.* 0.5 and 1 C), the effect of electrochemical polarization is little, so the battery temperature is the main factor to influence the discharge voltage. This explains why the discharge voltage of 0.5 and 1 C at 50 °C is higher than that at 25 °C during the whole discharge process and the discharge voltage is relatively high for both temperatures. When the batteries are discharged at rates of 5, 10 and 15 C, the electrochemical polarization becomes the main factor to influence the discharge voltage, which leads to an obviously low discharge plateau voltage. The discharge plateau voltage also decreases with the increase in discharge rate.

The battery temperature would not be increased immediately to an enough high temperature at the initial stage with high rate discharge (*e.g.* 5, 10 and 15 C). A appropriate high temperature could enhance the lithium-ion diffusion rate in solid phase and electrolyte, which results in the higher plateau voltage at 50 °C than that at 25 °C at the initial discharge stage. The battery temperature gradually increases during the large current discharge process. It can be seen from Figs. 8 and 11 that the battery temperature reaches about 35 and 58 °C, respectively, when the discharge plateau voltage at 25 °C is higher than that at 50 °C. A temperature as high as 58 °C may induce some other reactions and change of the battery materials except for enhancing the lithium-ion diffusion rate. For example, the thermal decomposition of the electrolyte and the deposition of electrolyte decomposition products on the surface of the graphite are more severe with the increase in battery temperature. The Ni, Co, and Mn dissolution also might occur in the electrolyte at higher temperature. Except the common surface components, the Ni, Co, and Mn metal might be deposited on the graphite surface [22]. The battery temperature is higher at the later high-rate discharge stage, so the formation of SEI is one of the reasons why the polarization becomes larger at later discharge stage. The formed SEI also

raises the polarization from the beginning of the following charge-discharge process, which leads to the decrease of discharge voltage plateau with the increase in cycle number and the relatively bad cycling property for high-rate discharge at 50 °C. Another change may be some structure transformation from the hexagonal to spinel phase. The hexagonal to spinel phase transformation is promoted by the delithiation state, higher temperature and Ni, Co, and Mn metal deposition on the graphite surface [33]. The spinel phase is known to have lower electrochemical activity (i.e. lower discharge voltage and lower capacity) than the hexagonal one. So it may be possible for the growth of the cubic spinel phase on the surface of the hexagonal at higher temperature and partly delithiated state of the cathode [34]. Thus, when the temperature is increased to 58 °C, the effects of elevated temperature not only offsets the increase of lithium-ion diffusion rate, but also leads to further increase of the electrochemical polarization. So the discharge plateau voltage of batteries at 50 °C is lower than that at 25 °C at the latter discharge stage.

Fig. 14 shows the discharge capacity at discharge rate of 10 C, the capacity of constant current (CC) charge with various charge rates, and the capacity of constant voltage (CV) charge of batteries during 100 cycles. The capacity retention of batteries after 100 cycles with charge rates of 1, 3, 5 and 8 C and discharge rate of 10 C is 97.10, 97.05, 95.56 and 95.00%, respectively. This indicates that the batteries show excellent cycle performance at various charge rates of 1, 3, 5 and 8 C and discharge rate of 10 C.

The average value of the portion of CC-charge capacity during 100 cycles at various charge rates of 1, 3, 5 and 8 C as shown in Table 1 is respective 92.73, 84.04, 76.24 and 54.98%. For a given battery system, the portion of CC-charge or CV-charge capacity is defined as the ratio of the CC-charge or CV-charge capacity to the sum of total charge capacities [35]. The value of the portion of CV-charge capacity reflects a charging rate, while an increase in the value corresponds to a loss in the capacity and power. So the battery would suffer an accelerated capacity fading due to high polarization caused by the local imbalance between the cell reac-

**Table 1**

The average charge and discharge capacity of 100 cycles with various charge rate and 10 C discharge rate obtained from Fig. 14

| Charge current (mA) | Capacity of CC-charge (mAh) | Capacity of CV-charge (mAh) | Capacity of total charge (mAh) | Capacity of discharge at 10 C (mAh) | Portion of CC-charge (%) | Coulombic efficiency (%) |
|---|---|---|---|---|---|---|
| 1300.00 | 1141.90 | 89.59 | 1231.49 | 1229.60 | 92.73 | 99.85 |
| 3900.00 | 1035.06 | 196.60 | 1231.66 | 1227.91 | 84.04 | 66.69 |
| 6500.00 | 939.97 | 293.00 | 1232.97 | 1224.94 | 76.24 | 99.35 |
| 10400.00 | 681.70 | 558.30 | 1240.00 | 1222.46 | 54.98 | 98.59 |

tion and the ionic diffusion on the electrolyte–electrode interface, resulting in metallic lithium plating on the anode or overcharge on the cathode [35]. It can be seen from Fig. 14 that the CC-charge and CV-charge capacities at various charge rates of 1, 3, 5 and 8 C almost do not change with the increase of the cycle number, which proves that the above phenomena almost do not exist in these batteries.

The average value of coulombic efficiency at charge rates of 1, 3, 5 and 8 C and discharge rate of 10 C during 100 cycles is 99.85, 99.69, 99.35 and 98.59%, respectively. It can be seen that the value slightly decreases with the increase of charge current. The battery temperature also gradually increases during higher current charging, which results in irreversible decomposition reactions of the electrolyte and leads to the decrease of coulombic efficiency. Overall, the above results show that the batteries exhibit superior high-current charge/discharge performance.

## 4. Conclusions

The commercial 18650 $Li(Ni_{1/3}Co_{1/3}Mn_{1/3})O_2$/graphite high power batteries were prepared and their electrochemical performance at temperatures of 25 and 50 °C was studied. It has been found that the EIS of the power batteries varies with the SOC of batteries. The $R_{ct}$ and $R_{sei}$ decrease as SOC increases from 0 to 60%; whereas they increase as SOC increases from 60 to 100%. The discharge plateau voltage of batteries is influenced by discharge rate and temperature. The discharge plateau voltage of batteries decreases greatly with the increase in discharge rate at both 25 and 50 °C. The plateau voltage for 0.5 and 1 C rate at 50 °C is slightly higher than that at 25 °C during the whole discharge process. The plateau voltage for 5, 10 and 15 C rate at 50 °C is higher than that at 25 °C at the initial discharge stage, whereas it is lower at the later discharge stage. The high power batteries show excellent rate performance with a discharge rate of 15 C and superior cycling performance with a discharge rate of 10 C at 25 °C. The higher temperature does not influence the battery discharge capacity and cycling performance at lower discharge rates (*e.g.* 0.5, 1, and 5 C); whereas it results in low discharge capacity at higher discharge rates (*e.g.* 10 and 15 C) and bad cycling performance at discharge rate of 10 C. The batteries also exhibit superior high-current charge/discharge performance.

## References

[1] I.B. Weinstock, J. Power Sources 110 (2002) 471.
[2] A.M. Andersson, D.P. Abraham, R. Haasch, S. MacLaren, J. Liu, K. Amine, J. Electrochem. Soc. 149 (2002) A1358.
[3] J. Jiang, J.R. Dahn, Electrochem. Commun. 6 (2004) 39.
[4] T. Ohsaki, T. Kishi, T. Kuboki, N. Takami, N. Shimur, Y. Sato, M. Sekino, A. Satoh, J. Power Sources 146 (2005) 97.
[5] D.D. MacNeil, J.R. Dahn, J. Electrochem. Soc. 149 (2002) A912.
[6] Y. Shigematsu, S.-I. Kinoshita, M. Ue, J. Electrochem. Soc. 153 (2006) A2166.
[7] Y. Baba, S. Okada, J.-I. Yamaki, Solid State Ionics 148 (2002) 311.
[8] J.R. Dahn, E.W. Fuller, M. Obrovac, U.v. Sacken, Solid State Ionics 69 (1994) 265.
[9] M. Wohlfahrt-Mehrens, C. Vogler, J. Garche, J. Power Sources 127 (2004) 58.
[10] H.-W. Ha, N.J. Yun, K. Kim, Electrochim. Acta 52 (2007) 3236.
[11] M.M. Thackeray, M.F. Mansuetto, J.B. Bates, J. Power Sources 68 (1997) 153.
[12] K. Amine, J. Liu, I. Belharouak, S.-H. Kang, I. Bloom, D. Vissers, G. Henriksen, J. Power Sources 146 (2005) 111.
[13] M.-R. Yang, W.-H. Ke, S.-H. Wu, J. Power Sources 146 (2005) 539.
[14] C.W. Kima, M.H. Lee, W.T. Jeong, K.S. Lee, J. Power Sources 146 (2005) 534.
[15] S. Zhang, Electrochim. Acta 52 (2007) 7337.
[16] C. Deng, L. Liu, W. Zhou, K. Sun, D. Sun, Electrochim. Acta (2007).
[17] M.C. Smart, J.F. Whitacre, B.V. Ratnakumar, K. Amine, J. Power Sources 168 (2007) 501.
[18] W. Lu, J. Liu, Y.K. Sun, K. Amine, J. Power Sources (2007) 212.
[19] I. Belharouak, Y.-K. Sun, J. Liua, K. Amine, J. Power Sources 123 (2003) 247.
[20] K.M. Shaju, P.G. Bruce, J. Power Sources 174 (2007) 1201.
[21] S. Zhang, X. Qiu, Z. He, D. Weng, W. Zhub, J. Power Sources (2006) 350.
[22] S.B. Jang, S.-H. Kang, K. Amine, Y.C. Bae, Y.-K. Sun, Electrochim. Acta 50 (2005) 4168.
[23] S.H. Park, C.S. Yoon, S.G. Kang, H.-S. Kim, S.-I. Moon, Y.-K. Sun, Electrochim. Acta 49 (2004) 557.
[24] H.-Y. Chang, C.-I. Sheu, S.-Y. Cheng, H.-C. Wu, Z.-Z. Guo, J. Power Sources 174 (2007) 985.
[25] K.M. Shaju, G.V.S. Rao, B.V.R. Chowdari, Electrochim. Acta 48 (2002) 145.
[26] Y. Wang, J. Jiang, J.R. Dahn, Electrochem. Commun. (2007) 2534.
[27] X. Liu, G. Zhu, K. Yang, J. Wang, J. Power Sources 174 (2007) 1126.
[28] S.S. Zhang, K. Xu, T.R. Jow, Electrochim. Acta 51 (2006) 1636.
[29] M. Itagaki, S. Yotsuda, N. Kobari, K. Watanabe, S. Kinoshita, M. Ueb, Electrochim. Acta 51 (2006) 1629.
[30] S.S. Zhang, K. Xu, T.R. Jow, Electrochim. Acta 49 (2004) 1057.
[31] S.S. Zhang, K. Xu, T.R. Jow, J. Power Sources 160 (2006) 1403.
[32] A. Xiao, W. Li, B.L. Lucht, J. Power Sources 162 (2006) 1282.
[33] X. Wang, T. Hironaka, E. Hayashi, C. Yamada, H. Naito, G. Segami, Y. Sakiyama, Y. Takahashi, K. Kibe, J. Power Sources 168 (2007) 484.
[34] Y. Ozawa, R. Yazami, B. Fultz, J. Power Sources 119-121 (2003) 918.
[35] S.S. Zhang, J. Power Sources 161 (2006) 1385.